Journal of Materials Chemistry A

Accepted Manuscript

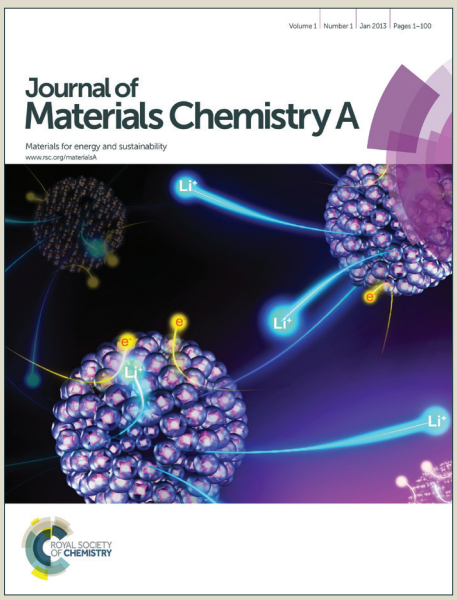

ROYAL SOCIETY OF CHEMISTRY

www.rsc.org/materialsA

Journal Name

RSCPublishing

COMMUNICATION

PbS Colloidal quantum dots as the effective hole transporter for planar heterojunction perovskite solar cells

Cite this: DOI: 10.1039/xoxxoooooox

Long Hu,[a] Weiwei Wang,[b] Huan Liu,[c] Jun Peng,[b] Hefeng Cao,[c] Gang Shao,[c] Zhe Xia,[a] Wanli Ma,[*b] and Jiang Tang,[*a]

Here, we applied colloidal quantum dots (CQDs) as an effective p-type hole-transporting material (HTM) for planar heterojunction perovskite solar cells. By tuning the size of PbS CQDs, we engineered the energy alignment of the valence and conduction band of this new HTM with the perovskite light harvester and achieved conversion efficiencies up to 7.5%. Absorption of PbS CQDs also extend the absorption spectrum of perovskite solar cells into the infrared.

Thanks to the ambipolar charge transport and high charge-carrier mobilities of organnometal halide perovskites, the "positive (p)-intrinsic (i)-negative (n)" thin-film heterojunction has recently emerged as a promising architecture for perovskite solar cells[1,2]. For example, Snaith et al. constructed planar p-i-n heterojunction perovskite solar cells having a 15.4% power conversion efficiency (PCE) where the vapour-deposited $CH_3NH_3PbI_{3-x}Cl_x$ film was sandwiched between the compact TiO_2 electron transporter and spiro-OMeTAD hole transporter.[3] Liu et al. achieved a PCE of 15.7% for the ITO/compact-ZnO/solution-processed $CH_3NH_3PbI_3$/spiro-OMeTAD/Ag.[4] Compared to the sensitized[5] and the meso-superstructured[6] solar cells using perovskites as light harvester, the planar "p-i-n" architecture[3] is simplified and offers a powerful new degree of freedom to the design and fabrication of high-efficiency perovskite solar cells because of versatile choices of both p- and n- charge transport and collection layers materials.

In most state–of–the–art high-efficiency perovskite solar cells, the hole transporter materials (HTMs), the most common of which is small molecular spiro-OMeTAD, play crucial roles although the hole conductor-free perovskite heterojunction solar cells were reported by several groups.[7-9] On the other hand, spiro-OMeTAD is expensive and requires p-type dopants and/or exposure to ambient atmosphere for optimal functioning at the risk of increasing production cost as well as degrading the perovskite, hence hindering their application in cost-effective perovskite solar cells. In this context, several HTM candidates besides the spiro-type arylamine such as alternative small molecules,[10,11] polymers,[12-19] and p-type inorganic semiconductors[20-23] have been reported, showing maximum PCEs of 12.8%, 16.2%, and 12.4%, respectively.

Among these HTMs, the inorganic materials are most cost-effective and have been widely employed in dye sensitized solar cells (DSSCs), however, only CuI,[20] CuSCN,[21] and NiO[22,23] have been reported to be effective HTMs in the field of perovskite solar cells. The selection of inorganic HTMs has to be based on suitable energy band alignment as well as processing compatibility with perovskites. Very recently, PbS quantum dots has been successfully introduced in the sensitized perovskite solar cells as a co-sensitizer together with $CH_3NH_3PbI_3$ to extend the absorption,[24,25] but the PbS CQDs as the HTM is still yet not reported to date. In this work, we demonstrate planar p-i-n heterojunction perovskite solar cells with maximum PCE of 7.5% that employ thin films of PbS CQDs as the HTM layer.

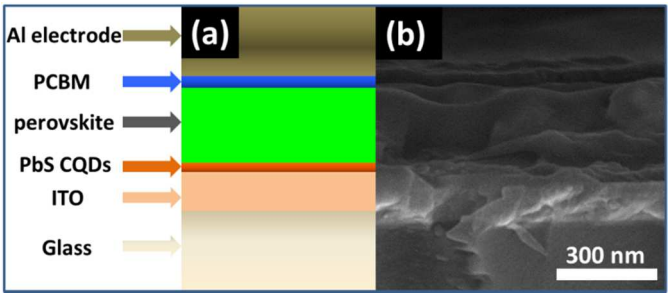

Fig. 1 (a) Schematic of device architecture. (b) Cross-sectional SEM image of the device.

As shown in Fig. 1a, we construct the planar PbS CQDs/$CH_3NH_3PbI_3$/PCBM device structure on indium-doped tin oxide (ITO)-coated glass front contact by spin-coating method and evaporate 100 nm of Al on top as the back contact. PbS CQDs of various sizes were synthesized through the reaction of Pb-oleate and bis(trimethylsilyl) sulfide (TMS) and deposited into p-type compact thin films following a modified published recipe.[26] 4 drops of PbS CQDs in hexane (8 mg/ml) were dropped onto ITO glass substrates, treated with tetramethylammonium hydroxide (TMAOH) methanol solution (10 mg/ml) and rinsed with methanol. We repeated this layer-by-layer process three

times and annealed the as-deposited samples at 70 °C in air for 12 hours. By using TMAOH for solid-state ligand exchange in ambient followed by air annealing to maximize oxygen binding and thus p-doping, we obtained highly robust p-type PbS CQDs films with the doping densities around 10^{18} cm^{-3}.[27] The PbS CQDs layer thickness is about 20 nm.

The $CH_3NH_3PbI_3$ perovskite layer was formed on top of the PbS CQDs film using two-step sequential deposition process inside a nitrogen-filled glovebox as previously reported,[5,23] followed by deposition of the n-type electron transporter PCBM which ensured the selective collection of electrons at the Al anode. Briefly, PbI_2 DMF solution (300 mg/ml) was spin-coated onto the PbS CQDs layer and baked on the hotplate at 70 °C for 30 min. When the PbI_2 seed layer cooled down to room temperature, it was immersed into a 10mg/ml CH_3NH_3I anhydrous isopropanol (IPA) solution (preheated to 50 °C), kept at 50 °C for 45 s, rinsed with absolute IPA solution for 10 s, and finally baked on 70 °C hotplate for 20 min to complete the formation of $CH_3NH_3PbI_3$ layer. The thickness of $CH_3NH_3PbI_3$ absorber layer is approximately 400 nm according to the cross-sectional scanning electron microscopy (SEM) image of the completed devices (Fig. 1b).

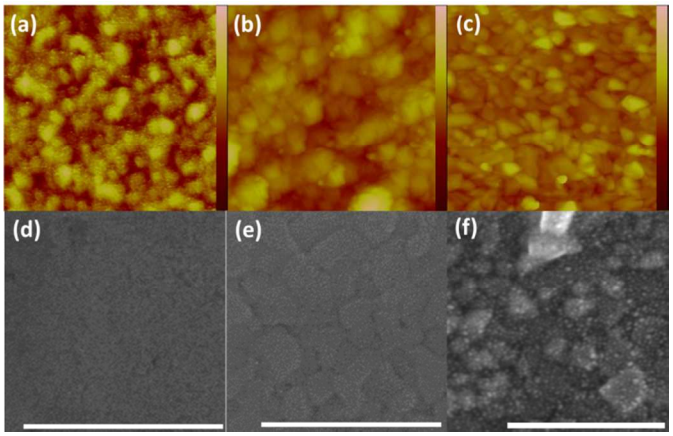

Fig. 2 Top-view SEM and AFM images of (a,d) the 1-PbS CQDs film; (b,e) the spin-coated PbI_2 layer on the 1-PbS layer; and (c,f) the $CH_3NH_3PbI_3$ film on the 1-PbS layer. The AFM image sizes are 5 × 5 μm and the scale bar is 0-10 nm, 0-100nm, and 0-300 nm for (a), (b) and (c), respectively. The scale bars for all SEM images are 500 nm.

For planar perovskite solar cells, flat and compact thin films of each layer are highly desirable for high efficiency. We characterized the film morphology and surface roughness of as-deposited PbS CQDs, PbI_2, and $CH_3NH_3PbI_3$ layers by Atomic force microscopy (AFM) with SEM (Fig. 2). The average surface roughness of PbS CQDs film was 0.84 nm, suggestive of a flat and compact HTM layer. The formation of larger PbI_2 crystals on top increased the surface roughness to 5.37 nm. After immersed into CH_3NH_3I, PbI_2 crystals immediately reacted with CH_3NH_3I and transformed into larger $CH_3NH_3PbI_3$ grains, increasing the film thickness and surface roughness (~10.58 nm). The $CH_3NH_3PbI_3$ film grown on the PbS CQDs HTM layer remained smooth and nonporous, a key parameter to avoid shunting paths that probably degrade the FF and V_{oc} in such planar devices.

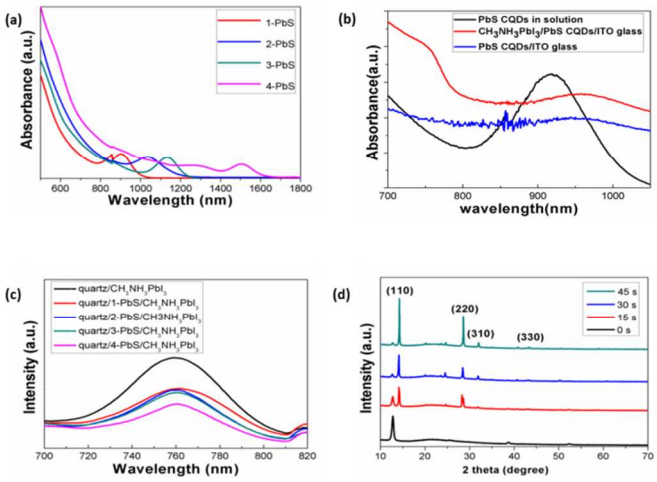

Fig. 3 (a) Absorption spectra of PbS CQDs of different sizes in solution. (b)Absorption spectra of PbS CQDs film and PbS CQDs/$CH_3NH_3PbI_3$ film. (c) Photoluminescence spectra of $CH_3NH_3PbI_3$ film on PbS CQDs film of different size (excited by 600 nm laser). (d) XRD patterns for the formation of the $CH_3NH_3PbI_3$ film; the number of seconds stand for the reaction time of PbI_2 dipping in CH_3NH_3I IPA solution.

With the benefit of a large excitonic Bohr radius of 18 nm and a low bulk energy bandgap of 0.41 eV, the bandgap of PbS CQDs can be widely tuned from 0.7 to 2.1 eV by facile size-tuning in dots synthesis. This distinct advantage enables us to investigate and understand the role of energy alignment of the perovskite/HTM interface in determining device parameters. We obtained PbS CQDs of different size by varying synthesis temperature and applied them as the HTM for comparison. Fig. 3a shows the absorption spectra of the smallest 1-, medium-sized 2- and 3-,as well as the largest 4-PbS CQDs, the first exciton adsorption peaks of which were at 890, 1050, 1150, and 1500 nm, approximately corresponding to energy bandgap values of 1.4, 1.2, 1.1 and 0.8 eV, respectively. We took the transmission electron microscope (TEM) to characterize as-synthesized 1-PbS CQDs (figure 1 in supporting imformantion). The average CQD size is approximately 3 nm, in accordance with previous report. We also measured the absorption spectra of PbS CQD film before and after the $CH_3NH_3PbI_3$ deposition (Fig. 3b). The excitonic peak of PbS CQD film still remained after $CH_3NH_3PbI_3$ deposition, confirming the preservation of quantum confinement of PbS CQDs. We then compared the 600 nm excited photoluminescence (PL) spectra of quartz/PbS CQDs/$CH_3NH_3PbI_3$ samples with quartz/$CH_3NH_3PbI_3$ and the results were shown in Fig. 3c. The $CH_3NH_3PbI_3$ band edge luminance at 760 nm was observed for all the samples but it could be quenched by the underlying PbS CQDs layer, indicative of effective charge transfer interactions between PbS CQDs and $CH_3NH_3PbI_3$, one of the prerequisites for PbS CQDs to be

effective HTM of perovskite solar cells. We applied X-ray Diffraction (XRD) measurements to study the structural evolution (Fig. 3d). The average grain size estimated from Scherrer Equation using XRD data was approximately 60 nm, consistent with the SEM observation. As the immersed time of PbI_2 film into CH_3NH_3I increased, diffraction peaks indexed to tetragonal $CH_3NH_3PbI_3$ enhanced; the prolonged treatment to 45 s resulted in strong diffraction peaks of $CH_3NH_3PbI_3$ with very small intensities of the PbI_2 diffraction peaks, suggestive of a quick and nearly complete transformation from PbI_2 to $CH_3NH_3PbI_3$ at elevated temperatures with trace amount of PbI_2 leftover that may be harmless.

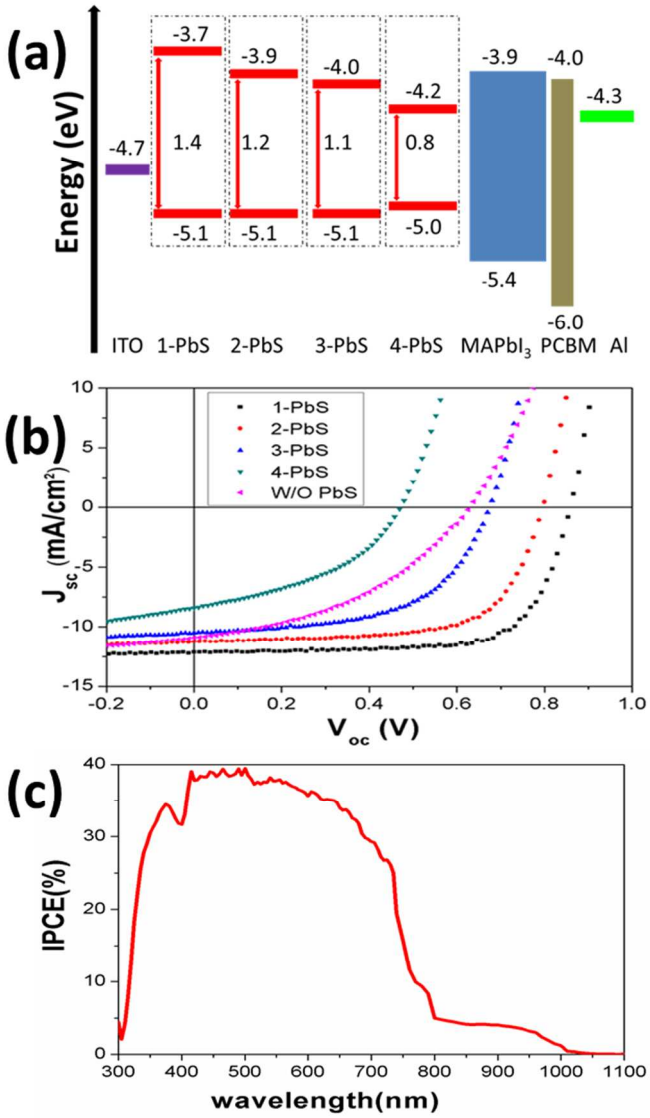

Fig. 4 (a) Energy level diagram of the corresponding materials used in our devices employing different PbS CQDs. (b) Current density-voltage characteristics of devices that employ PbS CQDs of various sizes as HTM. （c）The EQE spectra of photovoltaic device using 1-PbS.

The fact that the reduction in PL intensity is dependent on the size (bandgap) of PbS CQDs provides further evidence that the energy alignment of the PbS/ $CH_3NH_3PbI_3$ interface plays a crucial role on the charge transfer. According to the positions of the conduction bandedge (CB) and valence bandedge (VB) of the PbS CQDs,[30] we plotted the energy level diagram of the corresponding materials used in our devices that employed different PbS CQDs in Fig. 4a. The VB the PbS CQDs in this study all lies near -5.0~-5.1 eV and is shallow compared to the VB of $CH_3NH_3PbI_3$ (-5.4 eV); the ~0.4 eV valence band offset sufficiently favors hole injection from $CH_3NH_3PbI_3$ into PbS HTM. On the other hand, the CB become deeper as the PbS CQD size increased and it was deeper than the CB of $CH_3NH_3PbI_3$ (-3.9 eV) in the case of 3- and 4-PbS, showing a conduction band offset favouring the electron injection from $CH_3NH_3PbI_3$ into PbS. As a result, the largest 4-PbS led to maximum PL intensity reduction. On the contrary, the smallest 1-PbS had a CB shallow than -3.9 eV, thereby blocking the electron injection from $CH_3NH_3PbI_3$ into PbS and showed minimum PL quenching degree.

This picture of band alignment is further confirmed by the photovoltaic device performance measured under standard AM 1.5G illumination. As shown in Fig. 4b and Table I, the electron injection from $CH_3NH_3PbI_3$ was favored as the CB of PbS became deeper than that of into $CH_3NH_3PbI_3$, lowering both the photovoltage and photocurrent. As a result, the Voc, Jsc and PCE decreased monotonically as the PbS CQDs size increased. The smallest 1-PbS (890 nm-wavelength and 1.4 eV-bandgap) was found to be the most effective HTM owing to the shallowest CB and least light absorbing due to its largest bandgap, so that it could effectively block the undesired electron injection from $CH_3NH_3PbI_3$ in addition to favour the hole injection. The Voc, Jsc, FF and PCE were determined as 0.86 V, 12.1mA/cm^2, 72% and 7.5%, respectively, all of which were improved compared to the device without the PbS CQDs HTM layer. The FF may be further increased by intentionally enhanced p-type doping of PbS CQDs. It should be noted that we have also fabricated solar cells employing PbS CQDs as the absorber, that is, ITO glass/PbS CQDS/PCBM/Al. The device showed very poor power conversion efficiency of less than 0.5% (Table S1, supporting information). We further measured the external quantum efficiency (EQE) of perovskite solar cells using PbS CQDs whose absorption peak is at 932nm as HTM. As shown in Fig. 4c, the clear contribution from 800 nm to 1000 nm is originated from PbS CQD THE, confirming their additional role as light absorbers that further extend the absorption spectrum of $CH_3NH_3PbI_3$ solar cells into the infrared.

Table I. Device parameters of the solar cells that employ PbS CQDs HTMs of various badgaps.

P-type PbS	Absorption peak (nm)	Bandgap (eV)	V_{oc} (V)	J_{sc} (mA/cm^2)	FF (%)	PCE (%)
1-PbS	890	1.4	0.86	12.1	72	7.5
2-PbS	1050	1.2	0.78	11.2	67	5.7
3-PbS	1150	1.1	0.67	10.5	57	4.0
4-PbS	1500	0.8	0.48	8.5	42	1.7
W/O PbS	/	/	0.63	10.9	37	2.6

In summary, we constructed planar heterojunction perovskite solar cells employing colloidal quantum dots as effective hole-transporting materials. Owing to the quantum confinement effect, we engineered the band alignment of the $CH_3NH_3PbI_3$/CQDs HTM interface through size control of PbS CQDs. The hole injection from $CH_3NH_3PbI_3$ into PbS CQDs is favored by the shallow valence bandedge of PbS CQDs compared to $CH_3NH_3PbI_3$; the electron injection could be blocked as long as the conduction bandedge position of PbS CQDs is higher compared to $CH_3NH_3PbI_3$, which could be achieved by decreasing the PbS CQDs size. The device based on this new hole transporting material showed optimized power conversion efficiency of 7.5% with their absorption extend to 1000 nm thanks to the absorption of PbS CQD HTM. The availability of various CQDs materials combined with their w solution-processablity and absorption extension could offer a versatile and cost-effective platform to understand and optimize perovskite solar cells.

The research described here has received funding from the National Natural Science Foundation of China (NSFC 61274055, 61322401), the director fund of Wuhan National Laboratory for Optoelectronics, the "National 1000 Young Talents" project, the Program for New Century Excellent Talents in University (NCET-12–0216), and the 973 Program of China (2011CBA00703). We thank the Analytical and Testing Center of HUST and the Center for Nanoscale Characterization and Devices of WNLO for the characterization support. We would also like to acknowledge Innovative Technology and Beijing Technol Science Co. Ltd. for glovebox and thermal evaporator technical assistance, respectively.

Notes and Reference

a Wuhan National Laboratory for Optoelectronics, Huazhong University of Science and Technology,1037 Luoyu Rd., Wuhan, Hubei 430074, China

Electronic mail: jtang@mail.hust.edu.cn.

b Institute of Functional Nano&Soft Materials (FUNSOM), Soochow University, Suzhou, Jiangsu 215123, China

Electronic mail: wlma@suda.edu.cn

c School of Optical and Electronic Information, Huazhong University of Science and Technology, 1037 Luoyu Rd., Wuhan, Hubei 430074, China

1 G. Hodes, *Science,* 2013, **342**, 317.
2 H. J. Snaith, *J. Phys. Chem. Lett*., 2013, **4**, 3623.
3 M. Liu, M. B. Johnston, and H. J. Snaith, *Nature,* 2013, **501**, 395.
4 D. Liu and T. L. Kelly, *Nat. Photonics,* 2014, **8**, 133.
5 J. Burschka, N. Pellet, S. J. Moon, R. Humphry-Baker, P. Gao, M. K. Nazeeruddin, and M. Gratzel, *Nature,* 2013, **499**, 316.
6 M. M. Lee, J. Teuscher, T. Miyasaka, T. N. Murakami, and H. J. Snaith, *Science,* 2012, **338,** 643.
7 L. Etgar, P. Gao, Z. Xue, Q. Peng, A. K. Chandiran, B. Liu, Md. K. Nazeeruddin, and M. Gratzel, *J. Am. Chem. Soc*., 2012, **134**, 17396.
8 Z. Ku, Y. Rong, M. Xu, T. Liu, and H. Han, *Sci. Rep*., 2014, **3**, 3132.
9 J. Shi, Y. Luo, H. Wei, J. Luo, J. Dong, S. Lv, J. Xiao, Y. Xu, L. Zhu, X. Xu, H. Wu, D. Li, and Q. Meng, *ACS Appl. Mater. Interfaces,* 2014, **6**, 9711.
10 N. J. Jeon, J. Lee, J. H. Noh, M. K. Nazeeruddin, M. Gratzel, and S. I. Seok, *J. Am. Chem. Soc*., 2013, **135**, 19087.
11 P. Qin, S. Paek, M. I. Dar, N. Pellet, J. Ko, M. Gratzel, and M. K. Nazeeruddin, *J. Am. Chem. Soc*., 2014, **136**, 8516.
12 B. Cai, Y. Xing, Z. Yang, W. H. Zhang, and J. Qiu, *Energy Environ. Sci*., 2013, **6**, 1480.
13 J. H Noh, S. H. Im, J. H. Heo, T. N. Mandal, and S. I. Seok, *Nano Lett*., 2013, **13**, 1764.
14 J. H. Heo, S. H. Im, J. H. Noh, T. N. Mandal, C. S. Lim, J. A. Chang, Y. H. Lee, H. J. Kim, A. Sarkar, Md. K. Nazeeruddin, M. Gratzel, and S. I. Seok, *Nat. Photonics,* 2013, **7**, 486.
15 P. Docampo, J. M. Ball, M. Darwich, G. E. Eperon, and H. J. Snaith, *Nat. Commun*., 2013, **4**, 2761.
16 B. Conings, L. Baeten, C. D. Dobbelaere, J. D'Haen, J. Manca, and H. G. Boyen, *Adv. Mater*., 2014, **26**, 2041.
17 Y. S. K, J. Lim, H. J. Yun, Y. H. Kim, and T. Park, *Energy Environ. Sci*., 2014, **7,** 1454.
18 S. Ryu, J. H. Noh, N. J. Jeon, Y. C. Kim, W. S. Yang, J. Seoa, and S. I. Seok, *Energy Environ. Sci*., 2014, DOI: 10.1039/c4ee00762j.
19 N. J. Jeon, J. H. Noh, Y. C. Kim,W. S. Yang, S. Ryu, and S. I. Seok, Nat. Mater., 2014, DOI: 10.1038/nmat4014.
20 J. A. Christians, R. C. M. Fung, and P. V. Kamat, *J. Am. Chem. Soc*., 2014, **136**, 758.
21P. Qin, S. Tanaka, S. Ito, N. Tetreault, K. Manabe, H. Nishino, M. K. Nazeeruddin, and M. Gratzel, *Nat. Commun*., 2014, **5**, 3834.
22 J. Y. Jeng, K. C. Chen, T. Y. Chiang, P. Y. Lin, T. D. Tsai, Y. C. Chang, T. F. Guo, P. Chen, T. C. Wen, and Y. J. Hsu, *Adv. Mater*., 2014, **26**, 4107.
23 L. Hu, J. Peng, W. Wang, Z. Xia, J. Yuan, J. Lu, X. Huang, W. Ma, H. Song, W. Chen, Y. B. Cheng, and J. Tang, *ACS Photonics,* 2014, **1**, 547.
24 G. Seo, J. Seo, S. Ryu, W. Yin, T. K. Ahn, and S. I. Seok, *J. Phys. Chem. Lett*., 2014, **5**, 2015.
25 L. Etgar, P. Gao, P. Qin, M. Graetzel, and M. K. Nazeeruddin. *J. Mater. Chem*. A, 2014, DOI: 10.1039/c4ta02711f.
26 J. Tang, K. W. Kemp, S. Hoogland, K. S. Jeong, H. Liu, L. Levina, M. Furukawa, X. Wang, R. Debnath, D. Cha, K. W. Chou, A. Fischer, A. Amassian, J. B. Asbury, and E. H. Sargent, *Nat. Mater.,* 2011, **10**, 765.
27 J. Tang, H. Liu, D. Zhitomirsky, S. Hoogland, X. Wang, M. Furukawa, L. Levina, and E. H. Sargent, *Nano Lett*., 2012, **12**, 4889.

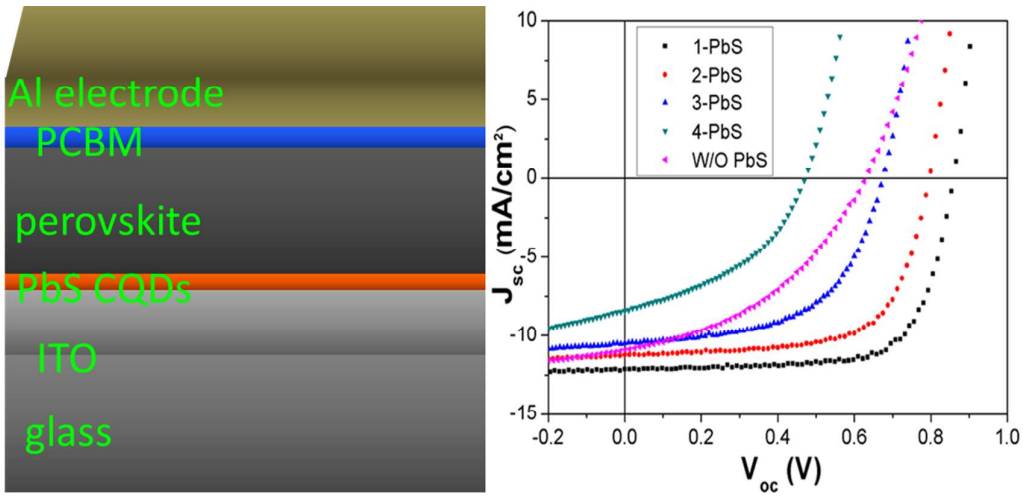

The planar heterojunction perovskite solar cells was constructed with PbS Colloidal quantum dots (CQDs) as the effective hole transporter , and we tuned the energy level of PbS CQDs to optimize the devices performance.